Calculation of self-consistent potentials for substitutionally disordered systems with application to the Ag_x-Pd_{1-x} alloy series

H. Winter
Kernforschungszentrum Karlsruhe, Institut für Technische Physik, 7500 Karlsruhe, Postfach 3640, Federal Republic of Germany

G. M. Stocks
Oak Ridge National Laboratory, Metals and Ceramics Division, P.O. Box X, Oak Ridge, Tennessee 37830
(Received 1 June 1982)

Previous Korringa-Kohn-Rostoker coherent-potential-approximation electronic-structure calculations for substitutionally random alloys have been based on *ad hoc* potentials. The lack of procedures suitable to provide self-consistent, parameter-free potentials prevented computations for systems consisting of dissimilar atoms and is also the reason why quantities like, for example, cohesive energies or lattice constants, have not so far been evaluated for systems of similar constituents. We present in full detail a generally applicable scheme devised for calculating the self-consistent electronic structures of substitutionally disordered systems. Its feasibility is demonstrated by presenting the results obtained for the Ag_xPd_{1-x} alloy series. They are compared with those of former non-self-consistent calculations which use Mattheiss prescription potentials and the $\alpha=1$ Slater exchange, whereas the von Barth—Hedin expression is employed in our work. The differences are perceptible and have to be understood as combined self-consistency and exchange-correlation effects.

I. INTRODUCTION

The application of the one-particle approach to the treatment of electrons in condensed matter requires some approximation for the effective-Coulomb interaction. Usually the local-density-functional approach (LDFA) is used.[1,2] The Coulomb interaction in the LDFA is written as the sum of the direct potential V^d as seen by a given electron due to the average charge distribution in the system and the exchange-correlation part V_{xc}. V_{xc}, at a given position depends only on the local-charge and spin-charge densities in that approach. The application of the LDFA can be justified from a theoretical point of view for systems in which the spatial charge-density variation is smooth. As this requirement is not met in all regions within a solid there is no *a priori* justification for the application of this scheme to such a system. Its merits and limitations therefore can only be recognized by comparing the values of calculated physical quantities to experiment. The request for maximum precision in the involved computations therefore bears not only practical but also principal significance. A basic demand in this context is that self-consistency of the calculations with respect to the one-particle potential should be obtained; that is to say, the input potential to the computation of quantities like energy eigenvalues, densities of states, etc., should be the same as the output potential as constructed with the help of those quantities. In fact, before the advent of reliable self-consistent band-structure calculations for ordered solids expressions for V_{xc} which contained adjustable parameters had to be used in many cases. The best-known example for this is the Slater $\rho^{\frac{1}{3}}$ expression with an adjustable prefactor α. In many applications based on non-self-consistent computations a value of 1 had to be chosen for α in order to get the best possible agreement between theory and experiment even in cases of high electronic densities where theory would have rather suggested values near $\frac{2}{3}$. The present state of the art of self-consistent electronic structure calculations for ordered solids, however, is so high that the expressions evaluated are fully parameter-free and remaining discrepancies between theory and experiment can genuinely be attributed to many body effects for many quantities. On the other hand, only due to the high standard of the practical calculations the amazingly wide applicability of the one-particle approach has been revealed.

In the case of disordered systems the situation is more complicated. Owing to the lack of Bloch symmetry it is much harder to perform reasonable

electronic-structure calculations. In addition, because some configurational averaging is involved in the computation of any physical quantity accessible to experiment approximations in addition to those connected with the single-particle picture enter any theory concerned with disordered solids. In order to test the validity of the alloy theory used and to get the best possible results for physical quantities within that theory it is therefore of great importance to work with good alloy potentials, which are self-consistent within the frame of the applied scheme.

In the present paper we consider configurationally disordered systems, the atoms of which are supposed to sit at the sites of a regular lattice. The most realistic theory for such systems has proven to be the Korringa-Kohn-Rostoker coherent-potential approximation (KKR-CPA).[3–6] It replaces the atoms of the alloy by a medium of effective scatterers. In the case of a A_xB_{1-x} alloy the sites of the effective medium are all characterized by the same single-site scattering matrices t_c which are determined by the requirement that, on the average, the effective medium should have the same scattering properties as the alloy. Given the alloy potentials, the t_c's have to be determined self-consistently for each electron energy, in order to meet the aforementioned CPA condition. Until recently the labor involved in the fulfillment of the CPA condition has prevented self-consistent calculations with respect to the alloy potential. As a consequence, KKR-CPA computations have been restricted to systems consisting of similar constituents, like Ag_xPd_{1-x} or Cu_xNi_{1-x} alloys, for which, due to the expected smallness of the charge transfer, potentials obtained by the use of the Mattheiss prescription[7] should lead to reasonable results. This assumption has been corroborated by the calculation of many physical quantities based on electronic-structure quantities as obtained in non-self-consistent KKR-CPA computations, like partial densities of states, Bloch spectral functions, Fermi surfaces, etc. Examples are the evaluation of the residual electrical resistivities of Ag_xPd_{1-x} alloys,[8] the interpretation of soft-x-ray-emission experiments,[9] the calculation of electron-phonon coupling parameters,[10] of positron-annihilation cross sections,[11] of angle-resolved photoemission cross sections,[12] etc.

Self-consistent alloy potentials even for systems like those cited above are not only desirable in order to improve the results for the aforementioned and similar quantities, but also in order to be able to calculate quantities which are likely to be very sensitive to the finer details of the electronic structure, like the cohesive energy, or to study whether there is any propensity for some short-range order in the system under consideration, etc. Only if self-consistency has been achieved, the question can be answered conclusively, if the KKR-CPA method itself is good enough to deal with such more subtle problems. Of paramount importance, however, is self-consistency for alloys consisting of atoms dissimilar in their atomic numbers and (or) their numbers of valence electrons. Without self-consistent potentials it is hard to make a theory for any of their physical properties.

The treatment of all the alloy problems so far precluded by the lack of self-consistency is now possible due to our method devised for doing full self-consistent KKR-CPA calculations. A short account of this work has been given in Ref. 13 and a description of the method, containing all the necessary information in a rather condensed form, together with its application to the $Ag_{0.2}Pd_{0.8}$ alloy has been published in Ref. 14.

In the present paper we discuss the formalism in full detail and present the results of self-consistent electronic-structure calculations for the whole Ag_xPd_{1-x} alloy series with the systems $Ag_{0.2}Pd_{0.8}$, $Ag_{0.5}Pd_{0.5}$, and $Ag_{0.8}Pd_{0.2}$ as examples. We compare our results with those of Ref. 6. For the case of the d-resonance positions in $Ag_{0.2}Pd_{0.8}$ we separate the effects caused by the use of different exchange-correlation potentials from those which are due to the achievement of self-consistency. Only the net effect will be discussed for other quantities.

Self-consistent potentials obtained by the use of our programs have already been applied to the calculation of the residual resistivities of Ag_xPd_{1-x} alloys and led to the improvement of the results over those based on the non-self-consistent potentials.[15] The self-consistent evaluation of the electronic structure of the Cu_xPd_{1-x} systems, which will be published elsewhere,[16] proved necessary to explain the disorder-order transition in those alloys as a consequence of the nesting properties of their Fermi surfaces.[17] The results of fully self-consistent KKR-CPA calculations are currently used to study clustering effects in Ag_xPd_{1-x} and Cu_xNi_{1-x} systems, to calculate cohesive energies and x-ray and ultraviolet photoelectron spectroscopy (XPS and UPS) spectra. A further interesting application, currently under way, is the investigation of magnetism in iron and nickel at finite temperatures both below and above the Curie point, where our method is applied to the disordered spin system of the valence electrons.

The present paper is organized as follows. In Sec. II we give a detailed discussion of the formalism, whereby the CPA is considered as the lowest-order approximation to a more general scheme for the treatment of substitutionally disordered alloys. In Sec. III we collect the points which show why the

cluster approach applied to an essential part of the procedure is able to treat systems big enough for providing reliable spatial electronic charge densities, which are used for the construction of the self-consistent potentials. Section IV is devoted to the discussion of the results obtained for the Ag_xPd_{1-x} alloy series, which perfectly back the statements made in the more general sections II and III. The paper concludes with a short summary.

II. THE FORMALISM FOR THE SELF-CONSISTENT CALCULATIONS

In the usual non-self-consistent treatment of the alloy problem the potentials around the atoms A and B, which go into the calculations via their single-site-scattering matrices t_A and t_B, respectively, are considered as input quantities and are obtained by using some sort of Mattheiss construction. The main effort to do a reasonable approximation to the configurational averaging is therefore put into the step, which calculates the scattering path operator T of the whole system out of the single-site scattering properties. This is usually done by solving the equation[18]

$$T^{i,j}=t^i\delta_{i,j}+\sum_{\bar{i}}{}' t^i g_0^{i\bar{i}} T^{\bar{i}j} \tag{1}$$

for T. $i,j,\bar{i}$ of Eq. (1) label the sites in the alloy and the $g_0^{i\bar{i}}$ are matrix elements of the free-electron Green's function. t^i is given by

$$t^i=\xi^{(i)}t_A+(1-\xi^{(i)})t_B\ , \tag{2}$$

where $\xi^{(i)}$ is 1 if i is occupied by an atom of sort A, and zero otherwise. The dependence of t_A and t_B on the particular configuration is neglected in this non-self-consistent treatment. In order to compare the theoretical results to experiment, the measured quantity has to be expressed by the quantities calculated by scattering theory and the configurational average taken at the end. So in principle (1) would have to be solved for all relevant configurations in the alloy system. On account of the large number of configurations involved and the lack of both point and Bloch symmetry clearly some approximation has to be introduced into the problem.

Instead of imposing some approximation on a perturbation-theory-based formulation, which hardly leads to both a physically intelligible and computational kind of theory, the use of CPA is a quite suggestive approach from a physical point of view. It gives an approximation to the configurationally averaged matrix elements of the scattering path operator $T^{A(B)}$, at a particular atom by replacing its environment in the alloy by an effective medium whose sites carry the single-site scattering matrices, t_c. $T^{A(B)}$ is easily obtained by solving this single-impurity problem and we obtain

$$T^{A(B)}=[1+T^c(t_{A(B)}^{-1}-t_c^{-1})]^{-1}T^c\ . \tag{3}$$

The evaluation of $T^{A(B)}$ implies the inversion of only a small matrix in any case. If the system has O_h symmetry and the maximum angular momentum, which has to be taken into account in an angular-momentum representation of the involved quantities, is $l=2$, (3) is merely an algebraic equation. In Eq. (3) T^c is the scattering path operator of the pure effective medium and has to be calculated by solving the equation

$$T^c=t_c+t_c g_0 T^c\ . \tag{4}$$

Relation (4) is the scattering equation of an ordered one-component solid.

At this stage, t_c is not yet specified. The CPA determines this quantity in such a way as to adjust the overall scattering properties of the effective medium to those of the alloy. The CPA condition, which assures that the average atom in the alloy causes no extra scattering when embedded into the effective medium, reads

$$cT^A+(1-c)T^B=T^c\ . \tag{5}$$

Here c is the concentration of the A atoms in the system. This relation is usually cast into an equation for t_c. By inserting (3) into (5) one obtains

$$t_c^{-1}=ct_A^{-1}+(1-c)t_B^{-1}+(t_c^{-1}-t_A^{-1})T^c(t_c^{-1}-t_B^{-1})\ . \tag{6}$$

Equations (5) and (6) have to be solved simultaneously for both t_c and T^c. The numerical treatment of this problem will be referred to as the CPA cycle in the following. By running through the CPA cycle for a sufficiently dense mesh of energy points the physical quantities of interest can be calculated within the non-self-consistent CPA approximation. The charge density at the average A or B site, e.g., may be obtained by exploiting its relation to the energy-integrated imaginary part of the single-particle Green's function[18]:

Here $\vec{\rho}$ is the spatial coordinate counted from site A. An equivalent formula holds for $\bar{n}^B(\vec{\rho})$. Z_L^A is a solution of the Schrödinger equation in the alloy potential $\bar{V}^A$ in the Wigner-Seitz cell of the average A atom in the alloy. $\bar{V}^A$ is assumed to be of muffin-tin form and L stands for the angular-momentum quantum numbers of Z.

In order to establish a formalism which is suitable to obtain self-consistency with respect to the alloy potentials we have to give a prescription for constructing potentials out of the charge densities determined by formula (7). In contrast to the ordered case this is not straighforward, because again some kind of configurations averaging is involved in this step. It should be on the same level as that applied to the scattering equation (1). For this purpose it is useful to devise a hierarchy of approximation to the alloy problem within which the CPA may be considered as the lowest-order one. This is done in the following way. The alloy is subdivided into two regions (Fig. 1): Region I contains the site whose scattering properties are to be calculated, whereas region II consists of the more distant sites outside region I. Whereas in region I a particular configuration of the atoms is considered, the atoms of region II are replaced by the scatterers of the effective medium. Similarly to Eq. (3) the scattering matrix of this system may be written in terms of the scattering matrix, T^c, of the effective medium as given by Eq. (4)

$$T=[1+T^c(t_{\mathrm{I}}^{-1}-t_c^{-1})]^{-1}T^c \ . \tag{8}$$

Computing T via Eq. (8) requires the inversion of a matrix whose dimension is determined by the number of atoms within region I and the maximum angular momenta taken into account. In general the single-site t matrices t_{I}, in region I are different for each site and depend on the given configuration. The CPA consists in restricting region I to just the central site and therefore is in fact the lowest-order approximation in the hierarchy of approaches which consist in using different sizes for region I.

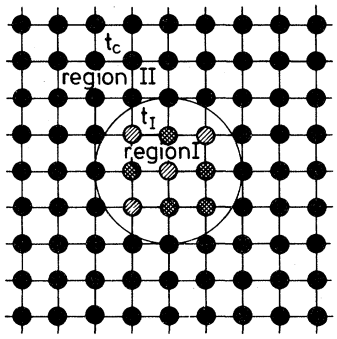

FIG. 1. Approach to the alloy problem by calculating the scattering path operator for the medium shown. Region II consists of the scatterers of the CPA effective medium. In region I we consider a special configuration with the shaded circles designating the A atoms and the cross-hatched circles designating the B atoms.

The prescription for the construction of the potential fitting into this scheme, now comes in in a natural way. It is based on the following charge densities. Within site i of region I the charge density $n_{\mathrm{I}}^{(i)}(\vec{\rho})$, used for the potential construction, is calculated with the use of Eqs. (8) and (7). We ascribe the concentration-weighed average $\bar{n}(\vec{\rho})$ of the charge densities at the average A and B atoms to the sites of region II:

$$\bar{n}(\vec{\rho})=c\bar{n}^{(A)}(\vec{\rho})+(1-c)\bar{n}^{(B)}(\vec{\rho}) \ . \tag{9}$$

A precise prescription for actually calculating $\bar{n}^{(A)}(\vec{\rho})$ and $\bar{n}^{(B)}(\vec{\rho})$ will be given below when we give a detailed description of the self-consistency procedure.

In terms of $n^{(i)}(\vec{\rho})$ and $\bar{n}(\vec{\rho})$ the potential $V^{(i)}$ at site i in region I corresponding to a given configuration is determined by the relation

$$V^{(i)}(\vec{\rho})=\sum_{i'\in \text{ region I}}\left[\int d\vec{\rho}\,'2n_{\mathrm{I}}^{(i')}(\vec{\rho}\,')\Big/|\vec{\rho}+\vec{\mathrm{R}}_i-\vec{\rho}\,'-\vec{\mathrm{R}}_{i'}'|-2Z^{(i')}/|\vec{\mathrm{R}}_i+\vec{\rho}-R_i'|\right]$$
$$+\sum_{i''\in \text{ region II}}\left[\int d\vec{\rho}\,'2\bar{n}(\vec{\rho}\,')\Big/|\vec{\rho}+\vec{\mathrm{R}}_i-\vec{\rho}\,'-\vec{\mathrm{R}}_{i''}|-2\bar{Z}/|\vec{\mathrm{R}}_i+\vec{\rho}-\vec{\mathrm{R}}_{i''}|\right]+V_{\mathrm{xc}}(n^{(i)}(\vec{\rho}))\ . \tag{10}$$

Here $Z^{(i')}$ is the nuclear charge at site i' and $\bar{Z}$ is a charge obtained in a way analogous to Eq. (9),

$$\bar{Z}=cZ^{(A)}+(1-c)Z^{(B)} \ . \tag{11}$$

In the following we use the muffin-tin approximation for $V^{(i)}(\vec{\rho})$ throughout. This amounts to replacing $n_{\mathrm{I}}^{(i)}(\vec{\rho})$ and $\bar{n}(\rho)$ by the charge densities displayed in Table I.

In close analogy to the procedure applied to the ordered case the muffin-tin potential is constructed most conveniently by some regrouping of these charge densities. For this purpose we define the total electronic charges contained in the muffin-tin spheres:

$$N_s^{(i)}=4\pi\int_0^{\mathrm{RMT}^{(i)}}\rho^2 d\rho n_s^{(i)}(\rho) \ , \tag{12a}$$

TABLE I. The construction of the charge densities for the computation of the alloy potential in muffin-tin form.

$n_{\mathrm{I}}^{(i)}(\vec{\rho})=$	$n_s^{(i)}(\rho)$:	the spherically averaged charge density	for $\vec{\rho}$ within the muffin-tin sphere of site i
	$\langle n^{(i)}\rangle$:	the spatially averaged interstitial charge density within the Wigner-Seitz cell of site (i)	for $\vec{\rho}$ outside the muffin-tin sphere but within the Wigner-Seitz cell (i)
$\bar{n}(\vec{\rho})=$		$\bar{n}_s=c\bar{n}_s^{(A)}(\rho)+(1-c)\bar{n}_s^{(B)}(\rho)$ with $\bar{n}_s^{(A)}$ and $\bar{n}_s^{(B)}$ the spherically averaged charge densities $\bar{n}^{(A)}$ and $\bar{n}^{(B)}$, respectively.	for $\vec{\rho}$ within the muffin-tin sphere of some site in region II
		$\langle\bar{n}\rangle=c\langle\bar{n}^{(A)}\rangle+(1-c)\langle\bar{n}^{(B)}\rangle$ with $\langle\bar{n}^{(A)}\rangle$ and $\langle\bar{n}^{(B)}\rangle$ the spatial averages over $\bar{n}^{(A)}$ and $\bar{n}^{(B)}$, respectively, in the interstitial regions.	for $\vec{\rho}$ in the interstitial parts of region II

$$\bar{N}=4\pi\int_0^{\mathrm{RMT}^{(i)}}\rho^2 d\rho\bar{n}_s(\rho)\ . \tag{12b}$$

Here $\mathrm{RMT}^{(i)}$ is the muffin-tin radius of site (i). The charge distribution now is written as the sum of the three contributions which are shown in Table II. In Table II $V_{\mathrm{MT}}^{(i)}$ is the volume of the muffin-tin sphere of site (i). $\bar{V}_{\mathrm{MT}}$ is the volume of the average muffin-tin sphere in the alloy. The part of the total potential, $V^{(i)}$, coming from the charge distribution (1) in Table II is easily calculated by noticing that, due to charge neutrality of this term at each site, $V^{(1)(i)}$ is determined by $n^{(1)(i)}$ and $Z^{(1)(i)}$ alone and is zero in the interstitial region. $V^{(2)}$ may be calculated by using the Ewald summation technique. Except for the contribution coming from $Z_{\mathrm{atom}}^{(3)(i)}$, which may easily be evaluated, the part of the potential due to (3) of Table II has to be evaluated numerically on a mesh of points within the Wigner-Seitz cell (i) and the averaging procedure necessary to obtain a muffin-tin form for the potential has to be performed afterwards. In many cases it is sufficient to approximate the potential outside the muffin-tin spheres by the average potential in the interstitial region of the whole system and to define its value as the muffin-tin zero. If necessary, the interstitial potentials are determined by averaging over the interstitial region of every Wigner-Seitz cell separately. In this case the interstitial potentials are site-dependent constants and the phase shifts are constructed by taking the logarithmic derivatives of the radial wave functions at the radii of the Wigner-Seitz rather than the muffin-tin spheres.

The formalism is now complete for the fully self-consistent treatment of the problem. In any case one starts out by restricting region I to just the central site. In many examples of almost complete randomness, e.g., for the $\mathrm{Ag}_x\mathrm{Pd}_{1-x}$ alloy system we are considering in this paper and the $\mathrm{Cu}_x\mathrm{Pd}_{1-x}$ system whose self-consistent electronic structure will be published elsewhere, this approximation is good enough for studying most of the properties of such systems. If it is not, or one is especially interested in short-range-order effects, the size of region I has to be increased after obtaining self-consistency under the aforementioned restriction. In the restricted case it is also possible to give a closed expression for the alloy potentials in terms of the charge densities of Table II. It reads

TABLE II. The regrouping of the contributions to the charge density in the alloy.

(1) $n_{\mathrm{electron}}^{(1)(i)}=n_s^{(i)}(\rho)-\langle\bar{n}\rangle$	for ρ within the muffin-tin sphere (i)	in region I
$=0$	for ρ outside the muffin-tin sphere (i)	in region I
$Z_{\mathrm{atom}}^{(1)(i)}=N_s^{(i)}-\langle\bar{n}\rangle V_{\mathrm{MT}}^{(i)}$		
$n_{\mathrm{electron}}^{(1)(i')}=\bar{n}_s(\rho)-\langle\bar{n}\rangle$	for (ρ) within the the muffin-tin sphere	in region II
$=0$	for (ρ) outside the muffin-tin sphere	in region II
$Z_{\mathrm{atom}}^{(1)(i')}=\bar{N}-\langle\bar{n}\rangle\bar{V}_{\mathrm{MT}}$		
(2) $n_{\mathrm{electron}}^{(2)}=\langle\bar{n}\rangle$	for the whole space	
$Z_{\mathrm{atom}}^{(2)(i)}=\bar{Z}-\bar{N}+\langle\bar{n}\rangle\bar{V}_{\mathrm{MT}}$	at any site	
(3) $n_{\mathrm{electron}}^{(3)(i)}=0$	for $\vec{\rho}$ within the muffin-tin radius	
$=\langle n^{(i)}\rangle-\langle\bar{n}\rangle$	in the interstitial region	at site (i) in region I
$Z_{\mathrm{atom}}^{(3)(i)}=(Z^{(i)}-\bar{Z})-(N_s^{(i)}-\bar{N})+\langle\bar{n}\rangle(V_{\mathrm{MT}}{}^{(i)}-\bar{V}_{\mathrm{MT}})$		in region I
$=0$		in region II

$$V^{(i)}(\vec{\rho})=V^{(1)}(\vec{\rho})^{(i)}+V^{(2)}(\vec{\rho})^{(i)}-Z^{(3)(i)}_{\text{atom}}/|\vec{\rho}| \tag{13}$$

and in muffin-tin approximation it is given by (compare the analogous expression for the muffin-tin potential for the case of an ordered system in Ref. 19)

$$V^{(i)}(\vec{\rho})=-\frac{2Z^{(i)}}{r}+8\pi\int_0^{\rho}\left[\frac{\rho'^2}{\rho}-\rho'\right]n_s^{(i)}(\rho')d\rho'+8\pi\int_0^{\text{RMT}(i)}\rho' n_s^{(i)}(\rho')d\rho'+V_{\text{xc}}(n_s^{(i)}(\vec{\rho}))$$

$$-V_{\text{xc}}(\langle\bar{n}\rangle)+\frac{C}{a}\langle\bar{n}\rangle(\bar{V}_{\text{WS}}-\bar{V}_{\text{MT}})\quad\text{for }\vec{\rho}\text{ within the muffin-tin sphere}$$

$$=0\quad\text{for }\vec{\rho}\text{ outside the muffin-tin sphere}. \tag{14}$$

Here (i) is either an A or a B atom.

In (14), $\bar{V}_{\text{WS}}$ is the volume of the average Wigner-Seitz cell in the alloy, a is its lattice constant, and C, the Madelung constant, is given by a number which depends on the crystal structure only.[20] In the case of a fcc structure, e.g., its value is 4.584 875 6. An average site-independent constant interstitial potential is used in formulas (13) and (14).

In the restricted case, described by formulas (13) and (14), there is a simple connection between the charge densities $n_s^{(i)}$ on the one side and $\bar{n}_s^{(A)}$, $\bar{n}_s^{(B)}$, $\langle\bar{n}^{(A)}\rangle$, and $\langle\bar{n}^{(B)}\rangle$ on the other:

$$\begin{aligned} &n_s^{(i)}=\bar{n}_s^{(A)},\quad\langle n^{(i)}\rangle=\langle\bar{n}^{(A)}\rangle \\ &\qquad\text{if region I is an } A \text{ atom}, \\ &n_s^{(i)}=\bar{n}_s^{(B)},\quad\langle n^{(i)}\rangle=\langle\bar{n}^{(B)}\rangle \\ &\qquad\text{if region I is a } B \text{ atom}. \end{aligned} \tag{15}$$

In the actual calculation the iteration process is initiated by gaining the charge densities of Table II via the superposition of atomic charge densities. This step is precisely defined by the equations (15). In the simplest case, formula (13), evaluated for (i) being occupied both by an A and a B atom, provides us with the potential. The solution of the corresponding Schrödinger equation yields the single-site scattering t matrices needed to run the CPA cycle, which consists in solving Eqs. (5) and (6) self-consistently. The output charge densities, $n_s^{(i)(\text{out})}$ and $\langle n^{(i)(\text{out})}\rangle$, are obtained by evaluating formulas (3) and (7) and by performing the averages as defined in Table I subsequently. The input charge densities for the next iteration are gained by admixing $n^{(i)\text{out}}$ to the input charge densities of the same iteration. The admixture factors may be chosen as large as 0.2 for systems with rather broad d resonances. In the application described in this paper, where extremely narrow d resonances come into play, it has to be restricted to a few percent in the first few iterations but may be raised to about 0.2 in the subsequent ones without running out of convergence. The number of iterations needed to achieve self-consistency is comparable to that necessary in ordered systems.

In the applications requiring an extension of region I, the next step consists in attaching the charge densities $\bar{n}_s$ and $\bar{n}$, and the single-site scattering matrices t_c, obtained in the computations described above, to the sites of region II. Keeping these boundary conditions fixed, Eqs. (7) and (8) have to be solved self-consistently for all relevant configurations in region I with both an A and a B atom in the center. Self-consistency in this step means that the potentials at the sites of region I, obtained with the use of the scattering path operator $T^{(n)}$ of the nth iteration yield single-site scattering matrices t_{I}, which are sufficiently close to those employed for the calculation of T via Eq. (8). The starting values of the charge densities for this kind of iteration procedure are of course those obtained in the above-mentioned restricted iteration process. The physical quantity in question is evaluated for each particular configuration of region I separately and the configurational average is taken at the end.

In spite of the far larger amount of expenditure necessary, if the second step is required, it should be manageable on the lines described above. Keeping in mind the successes of the CPA schemes in its simplest version, it is to be expected that the size of region I can be held fairly small in the cases where some amount of short-range order demands the performance of the second step, too.

III. THE APPLICATION OF THE CLUSTER APPROACH TO THE SELF-CONSISTENCY PROCEDURE

Much more numerical labor is involved in obtaining the self-consistent electronic structure of a substitutionally disordered substance than for an ordered system along the lines traced in the last chapter. The cause for this is that the self-consistency requirements, which have to be met simultaneously for both the single-site scattering matrix t_c of the effective medium and the alloy potentials require running through the two interrelated

self-consistency loops as described in the last section. It therefore would be desirable to perform at least some of the involved steps by using a method considerably faster than the full KKR-CPA. The most natural thing to do would be to approximate the extended effective medium by a finite cluster of sites when solving Eq. (4) for T^c. However, in order to obtain any meaningful results for the transition-metal alloy systems we are aiming at, the cluster must not be too small. Dealing with just one shell of atoms, surrounding the central site, e.g., would not be good enough. It would be inappropriate to neglect s- and p-wave scattering even in systems where d-wave scattering is highly dominant. On the other hand, it is well known that any unsophisticated approach to handle clusters quickly becomes unfeasible if it is necessary to deal with systems consisting of more than about 20 sites. However, by transcribing the fast symmetrized cluster approach of Ref. 21 to the alloy problem it becomes possible to deal with 100 and more sites, which makes the cluster method quite attractive for the type of problems we are concerned with here. The cause for the superiority of that approach of course is that the scattering equation (4) for the effective medium is equivalent to that of an ordered system with the full point symmetry of the crystal lattice. In our actual computations we do the whole self-consistency problem within the cluster approach handling systems with about 80 sites and obtain both the self-consistent alloy potentials and the partial and total densities of states from our cluster calculations.

The important point now is that the quality of these results can be checked by comparing them to those obtained by applying the full KKR-CPA to the problem. This is done in the following way. Using the self-consistent potentials as calculated in the cluster approach, we do one final KKR-CPA iteration step and compare the resulting charge densities to those of the cluster computations. It turns out that they coincide, as Figs. 3–5 show. This is not only the case for the Ag_xPd_{1-x} systems we are discussing in this paper but for other systems, too, for which we did computations. So it is well established that our cluster approach yields the same self-consistent alloy potentials as a full KKR-CPA applied throughout the iteration process would have. The same conclusion can be drawn by comparing

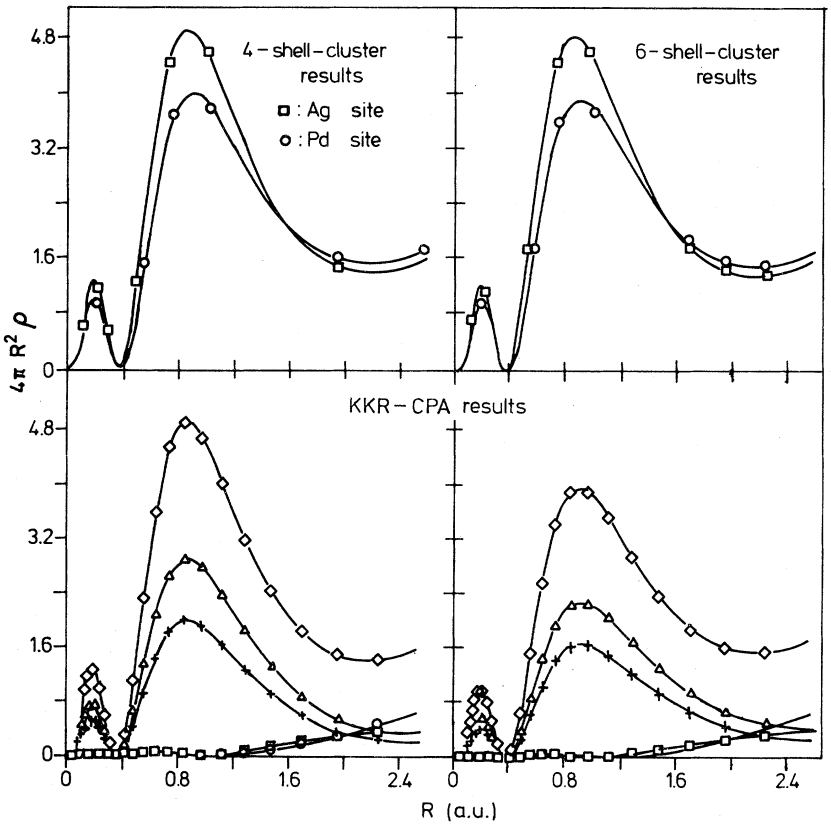

FIG. 2. The radial charge distributions for $Ag_{0.2}Pd_{0.8}$ as obtained from the DOS based on the non-self-consistent potentials. The symbols of the KKR-CPA results are explained in Fig. 3.

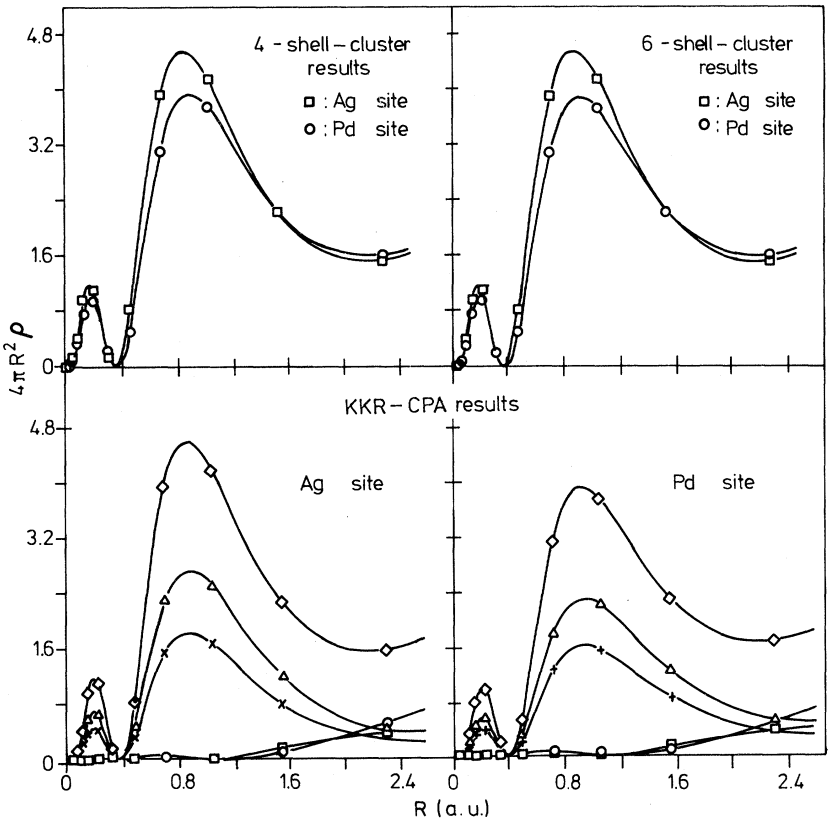

FIG. 3. The self-consistent radial charge distributions in $Ag_{0.2}Pd_{0.8}$. The graphs showing the KKR-CPA results display the individual contributions to the charge densities: □, s contribution; ○, p contribution; ×, e_g contribution; △, t_{2g} contribution; ◇, total charge-density.

the cluster to the KKR charge densities for runs based on the non-self-consistent Mattheiss prescription potentials (Fig. 2). The cluster densities of states of course do exhibit cluster-size-dependent differences in comparison to the exact results obtained with the KKR, the most marked difference being that the first mentioned are more structured. This feature, however, has practically no effect on energy-integrated quantities like charge densities. One cause for this is that the cluster puts the peaks on the right positions. By a further increase of the cluster size, which is quite feasible, it would be possible to bring the cluster-densities of states (DOS) still closer to those of the KKR, as a glance at Figs. 7—14 shows, where the results obtained for clusters with 43 and 79 sites, respectively, are displayed. The use of clusters containing fewer than about 40 sites is insufficient, at least for the alloys formed by transition-metal atoms, because the DOS curves gained from them, exhibit too much structure and therefore prevent the iteration procedure from becoming stable. Summing up, one can state that by doing a KKR-CPA band-structure calculation based on the self-consistent potentials as obtained with our cluster approach we are able to evaluate the self-consistent electronic structures of substitutionally random alloys on the same level of accuracy as that which would be achieved by applying the full KKR-CPA to each step involved in the procedure. The computer time required for our approach is tolerable and the calculations, discussed in this paper, have been performed both on an IBM-3033 and a Cray.

Because the ability to handle clusters consisting of about 100 sites is the clue to the possibility of obtaining self-consistency, it is worthwhile to show in detail how the speeding up in these computations is achieved. Most important in this connection is the choice of the most appropriate basis set of single-particle wave functions necessary to cast the scattering equation (4) into a matrix form. Usually the free-particle angular-momentum eigenfunctions centered around the different sites of the system are chosen. They are given by

$$Z_L^{(0)(i)}(\vec{\rho},\epsilon)=j_l(\sqrt{\epsilon}\,\rho)Y_L(\hat{\rho})\ . \tag{16}$$

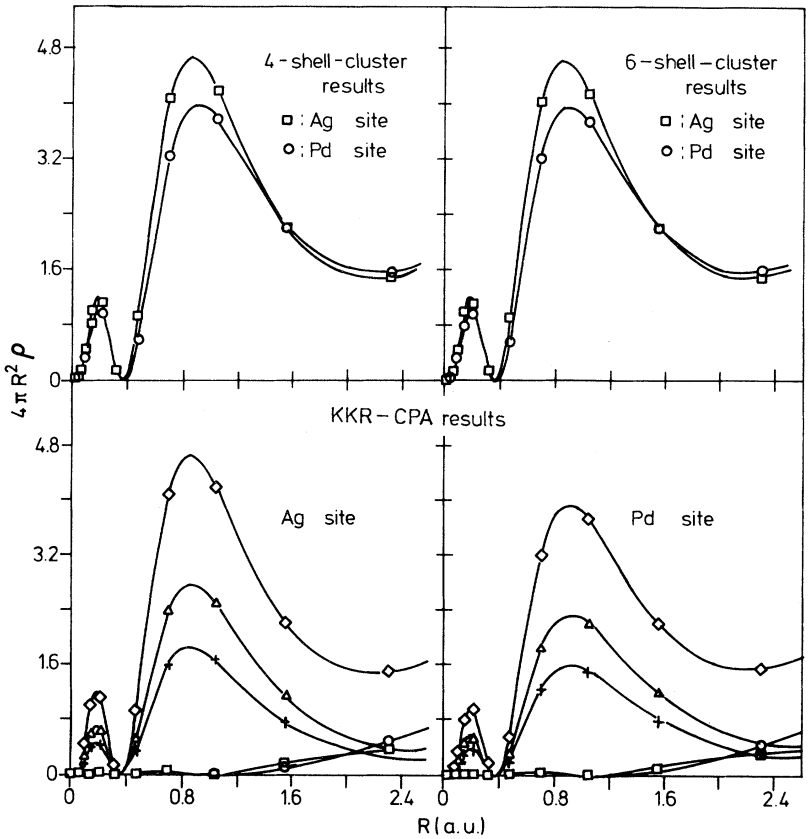

FIG. 4. The self-consistent radial charge distribution in $Ag_{0.5}Pd_{0.5}$. The meaning of the symbols is the same as explained in Fig. 3.

Here L stands for the angular-momentum quantum numbers, j_l is the spherical Bessel function, and Y_L are the real spherical harmonics. The coordinate $\vec{\rho}$ is counted from site (i).

In general the matrix elements of the scattering path operator T^c between any two of the functions defined in (16) are different from zero. Solving Eq. (4) in the representation (16) for T^c, therefore requires the setting up and inversion of a full matrix whose dimension D is given by

$$D(T^c)=N(l_{\max}+1)^2 \tag{17}$$

with N the number of sites in the cluster and $l_{\max}$ the maximum angular momentum taken into account. This gives a severe limitation to the manageable cluster size, because the time spent for the inversion goes roughly with the third power of D, and, also, the setting up of the big matrix, element by element, is rather time consuming.

Instead of (17) we use wave functions adapted to the point symmetry of the system. As is well known the matrix elements of T^c between states belonging to different representations of the point group, as well as between different basis states of the same representation, vanish. Using these basis states, the matrix

$$T^{c\,-1}=t_c^{-1}-g_0 \tag{18}$$

therefore is block-diagonal and T^c can be constructed by inverting those blocks separately.

The effect of this change of basis is best visualized by taking the 79-site cluster employed in the present calculations as an example: the effective medium, mimicking the Ag_xPd_{1-x} system, has fcc structure and O_h point symmetry, possessing 10 irreducible representations, M. Because the matrix elements of T^c are only needed at the central site and it is quite sufficient to put $l_{\max}$ equal to 2 we have to care for the blocks connected with four representations only. Their symbols and the dimensions of the corresponding blocks are displayed in Table III. In the nonsymmetrized treatment of the problem, on the other hand, the dimension of the matrix to be inverted would have been 711.

The symmetry-adapted states used in our calculations are constructed in the following way (compare Ref. 21 and Fig. 1). The atoms are grouped into

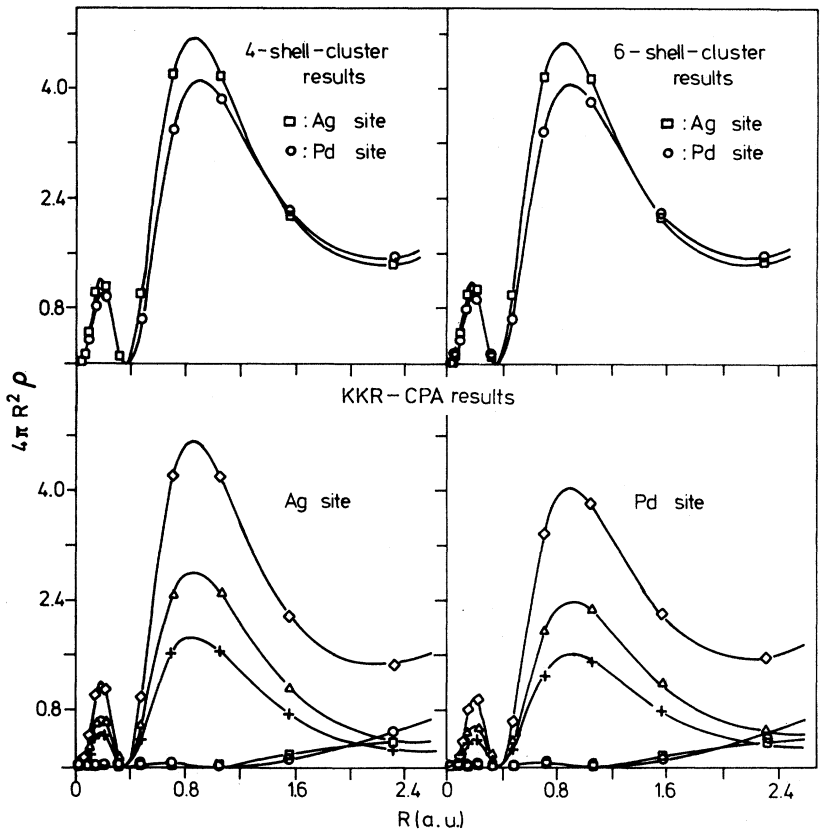

FIG. 5. The self-consistent radial charge distributions in $Ag_{0.8}Pd_{0.2}$. The meaning of the symbols is the same as explained in Fig. 3.

shells surrounding the point-symmetry center of the system. The positions of the atoms in a given shell are related to each other by symmetry operations. Each symmetrized state consists of a linear combination of single-site states, involving the sites of a particular shell s only, and may be written as

$$|M\nu\kappa\rangle = \sum_{\substack{i\in s \\ \mu}} C^{M\nu\kappa}_{\mu,i} |\lambda\mu,i\rangle \ . \tag{19}$$

Here $|M\nu\kappa\rangle$ is a basis state ν of the irreducible representation M. κ is a further label necessary to account for the multiplicity of the basis states. $|\lambda\mu i\rangle$ is an unsymmetrized state centered at site i and characterized by the two quantum numbers λ and μ. The $|\lambda\mu i\rangle$'s contained in a particular symmetrized state all carry the same quantum number λ. The states $|\lambda\mu i\rangle$, employed in the cases of O_h symmetry, are the cubic harmonics. By applying a Schmidt orthogonalization procedure to the $|M\nu\kappa\rangle$, the expansion coefficients C are constructed in such a way as to satisfy orthogonality relations. For additional details we refer to Ref. 21.

A further accelerating measure is introduced into the calculations for the step which sets up the symmetrized representation of $T^{c\,-1}$. It mainly consists in calculating the matrix elements of the free-particle Green's function g_0. They are given by

$$\langle M\nu\kappa \,|\, g_0 \,|\, M\nu\kappa'\rangle = \sum_{\substack{i\in s \\ \mu}} \sum_{\substack{i'\in s' \\ \mu'}} C^{M\nu\kappa}_{\mu,i} \langle \lambda\mu i \,|\, g_0 \,|\, \lambda'\mu' i'\rangle C^{M\nu\kappa'}_{\mu',i'} \ . \tag{20}$$

Most of the quantities entering formula (20), including the C's, are determined by the structure of the system alone. By comparison of (20) to formula (4.10) in Ref. 21 one sees that the $\langle \lambda\mu i \,|\, g_0 \,|\, \lambda'\mu' i'\rangle$ may be written as

$$\langle \lambda\mu i \,|\, g_0 \,|\, \lambda'\mu' i'\rangle = \sum_{l} \langle \lambda\mu i \,|\, \tilde{g}^{(l)}_0 \,|\, \lambda'\mu' i'\rangle h_l^{(+)}(\sqrt{\epsilon}\,|\,\vec{R}_{ii'}\,|\,)\sqrt{\epsilon} \tag{21}$$

TABLE III. The dimensions of the blocks in the symmetrized representation of the scattering-path operator for a six-shell cluster.

Symbols of the representations			Dimension of the corresponding block in the T matrix
1	A_g	Γ_1	24
2	T_{1u}	Γ_{15}	52
3	E_g	Γ_{12}	38
4	T_{2g}	Γ'_{25}	45

with $h_l^{(+)}$ a spherical Hankel function, ϵ the energy, and $|\vec{R}_{ii'}|$ the distance between the sites i and i'. The sum over l is restricted to a few terms for any combination of occurring quantum numbers λ and λ'. The first factor in (21) is again merely structural. A further simplification comes into play by noticing that the sum over the sites i of shell s in formula (20) may be omitted by multiplying (20) with the number of sites in shell s, summing over ν, the label of the basis states of M, and dividing by the dimension of M. i in Eq. (20) may be replaced by any site i_0 in shell s. In this way the number of Hankel functions with different arguments to be calculated is considerably reduced. By inserting Eq. (21) into Eq. (20) the matrix elements of g_0 may be written in the following way:

$$\langle M\nu\kappa \,|\, g_0 \,|\, M\nu\kappa'\rangle = \sum_{l,i'\in s'} B_{\kappa\kappa'}(l,i') \times\sqrt{\epsilon}\, h_l^{(+)}(\sqrt{\epsilon}\,|\vec{R}_{ii'}|)\,. \tag{22}$$

In our computations the energy- and lattice-constant-independent, merely structural, quantities are calculated once and then stored permanently. This short description of the way the cluster method is used in our computations should be sufficient to give a feeling why it is capable to deal with clusters consisting of more than 100 sites. In terms of the symmetrized states (19) the matrix equation (4) for the scattering path operator T^c reads

$$T^{cM}_{\kappa\kappa'} = t^M_{c\kappa,\kappa}\Delta_{\kappa,\kappa'} + \sum_{\bar\kappa} t^M_{c\kappa\kappa} g^M_{0\kappa\bar\kappa} T^{cM}_{\bar\kappa\kappa'}\,. \tag{23}$$

The labeling of the quantities setting up Eq. (23) is devised in such a manner as to exhibit the symmetry relations between their matrix elements as pointed out above.

The cluster approach is also very suitable for attaining self-consistency in the CPA cycle by applying the Newton-Ralphson procedure to Eq. (6), in order to obtain a new guess value $t_c^{(n)}$ for the t_c employed in the nth iteration, out of the input value $t_c^{(n-1)}$, to the $(n-1)$th iteration, on the one hand, and the value $T^{c(n-1)}$ of the scattering path operator as obtained in the $(n-1)$th iteration on the other. To that purpose we write $t_c^{(n)}$ as

$$t_c^{(n)} = t_c^{(n-1)} + \Delta t_c\,. \tag{24}$$

Δt_c is chosen such that $t_c^{(n)}$ satisfies the CPA condition Eq. (6) up to the first order in Δt_c. This leads to the relation

$$\begin{aligned}[1 - T^{c(n-1)}_\lambda (t_{c\lambda}^{(n-1)^{-1}} - t_{B\lambda}^{-1}) - (t_{c\lambda}^{(n-1)^{-1}} - t_{A\lambda}^{-1}) T^{c(n-1)}_\lambda]\Delta t_{c\lambda}^{-1} - \sum_{\lambda'} (t_{c\lambda}^{(n-1)^{-1}} - t_{A\lambda}^{-1}) \left[\frac{\delta T^c_\lambda}{\delta t^{-1}_{c\lambda'}}\right]^{(n-1)} (t_{c\lambda}^{(n-1)^{-1}} - t_{B\lambda}^{-1}) \\ = c t_{A\lambda}^{-1} + (1-c) t_{B\lambda}^{-1} + (t_{c\lambda}^{(n-1)^{-1}} - t_{A\lambda}) T^{(n-1)}_{c\lambda} (t_{c\lambda}^{(n-1)^{-1}} - t_{B\lambda}^{-1}) - t_{c\lambda}^{(n-1)^{-1}}\,.\end{aligned} \tag{25}$$

In Eq. (25) the matrix elements of the involved quantities are to be taken with respect to the states $|\lambda\mu i\rangle$ as introduced in Eq. (9) and i there is the central site. In the case of O_h symmetry and $l_{\max}=2$, which, for the sake of simplicity, is assumed in deriving (25), these matrix elements are diagonal in λ and independent of μ. At the central site the states $|M\nu\kappa\rangle$ are identical to the states $|\lambda\mu 1\rangle$ in this case.

The solution of (25) requires the calculation of the functional derivative of T^c with respect to t_c. By a functional derivation of Eq. (4) with respect to t_c we obtain

$$\frac{\delta T^c_\lambda}{\delta t^{-1}_{c\lambda'(\kappa')}} = -\sum'_{\kappa'} T^{c\lambda}_{1\kappa'} T^{c\lambda}_{\kappa' 1}\,. \tag{26}$$

In (26) the $T^{c\lambda}_{1\kappa'}$ are symmetrized matrix elements of T^c as defined in Eq. (23). $\kappa=1$ is the label for the involved states at the central site and the κ's only run over those states which are a linear combination of single-site states with quantum number λ'. The summation over the sites of the cluster involved in (26) is effected with negligible expenditure of time, and Eq. (25) is solved for Δt_c by inverting the small matrix on the lhs. Self-consistency with respect to the CPA cycle is attained after fewer than four iterations for most of the energy points. The full, energy-dependent, matrix elements g_0 of course, have to be set up only once per CPA cycle.

IV. RESULTS FOR THE SILVER-PALLADIUM ALLOY SYSTEM

We present the results of self-consistent electronic-structure calculations for the composi-

tions $Ag_{0.2}Pd_{0.8}$, $Ag_{0.5}Pd_{0.5}$, and $Ag_{0.8}Pd_{0.2}$, which have been performed by following the lines of Secs. II and III. In these computations we restrict ourselves to the CPA approximation; that is to say, region I consists of only one site. We applied the self-consistency procedure to clusters of both 43 (4 shells of atoms) and 79 (6 shells of atoms) sites in the $Ag_{0.2}Pd_{0.8}$ case and to 79-site clusters in the others. The maximum angular momentum taken into account was $l=2$ for each site. f scattering could easily be included if necessary. We constructed our potentials according to Eq. (14) and used the von Barth—Hedin expression for the exchange-correlation part V_{xc}.[22] The experience gained for V_{xc} is the same as for ordered systems: one of the merits of the self-consistency is that reasonable results can be obtained by utilizing physically well-founded exchange-correlation potentials, which contain no adjustable parameter. The non-self-consistent calculations of Ref. 6 on the other hand, which are based on Mattheiss prescription potentials, use the $\alpha=1$ Slater exchange in order to get better agreement with experiment.

For comparison we reproduce these results by using the same ad hoc potentials and refer to them as non-self-consistent calculations in the following. Furthermore, the number of iterations necessary to obtain convergence in the self-consistency procedure can be minimized by using these potentials as starting quantities. In the first four iterations we gained the input potentials to the ith iteration by mixing the input and output potentials of the $(i-1)$th iteration. We found that convergence can be speeded up by switching to the mixture of charge densities in the subsequent iterations. We also observed that the converged potentials of the $Ag_{0.2}Pd_{0.8}$ system lead to rapid convergence when used as input quantities to the computations for different concentrations. By comparing our results obtained with these two different kinds of starting potentials we conclude that they are independent of the initial guess, provided self-consistency has been achieved. Although the positions of the extremely narrow d resonances at the silver sites are very sensitive to the details of the charge distributions, admixture factors as large as 0.2 could be used in the third and the subsequent iterations and we attained self-consistency after typically eight to ten iterations. Self-consistency has been considered achieved as soon as the rms difference between the output potentials of two subsequent iterations fell below 10^{-5} Ry. This amounts to a shift in the silver d resonances, which are the most sensitive quantities, of less than 0.001 Ry.

In the first iteration the average t-matrix approximation (ATA) to the single-site t matrices t_c of the effective medium was taken as an input guess to the CPA cycle. In the subsequent iterations the self-consistent t_c's of the previous iteration have been used for this purpose. Convergence with respect to the CPA cycle has been attained after typically four iterations for each energy point in the first few iterations and this number has even been reduced for most of the energy points in the subsequent iterations, when the potentials were approaching their self-consistent values. Self-consistency with respect to the CPA cycles have been considered achieved as soon as the correction to the t_c's suggested by the Newton-Ralphson equation (25) fell below 0.01% of the computed values for any matrix element of t_c.

In order to stabilize the procedure the scattering path operator for about 180 energy points had to be determined. In this way the cluster approach not only provides self-consistent charge densities, potentials, and single-site scattering matrices but also partial and total densities of states. However, we should like to stress here again that only the single-site quantities as obtained by the cluster approach are really used in the determination of the electronic structure; quantities like the densities of states or, more generally, the one-particle Green's functions are obtained by the application of the full KKR-CPA to which the self-consistent potentials are the input quantities. The validity of our approach only depends on how near the charge densities as determined in our cluster approach are to those obtained by using the full KKR-CPA. This can easily be controlled and has been controlled in our calculations. The comparison of the four-shell-cluster to

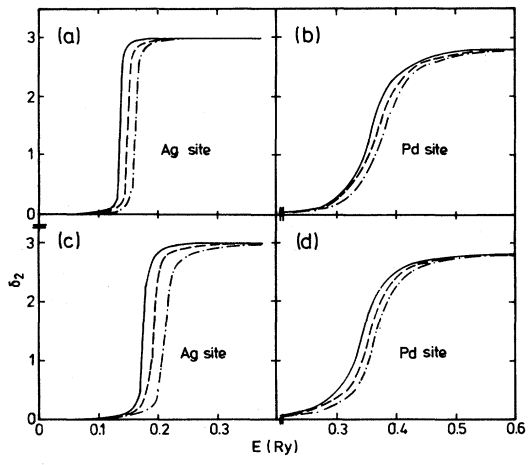

FIG. 6. The d phase shifts for the Ag_xPd_{1-x} alloys: dot-dashed curve, $Ag_{0.2}Pd_{0.8}$; dashed curve, $Ag_{0.5}Pd_{0.5}$; solid curve, $Ag_{0.8}Pd_{0.2}$. The non-self-consistent results are displayed in (a) and (b), the self-consistent results in (c) and (d).

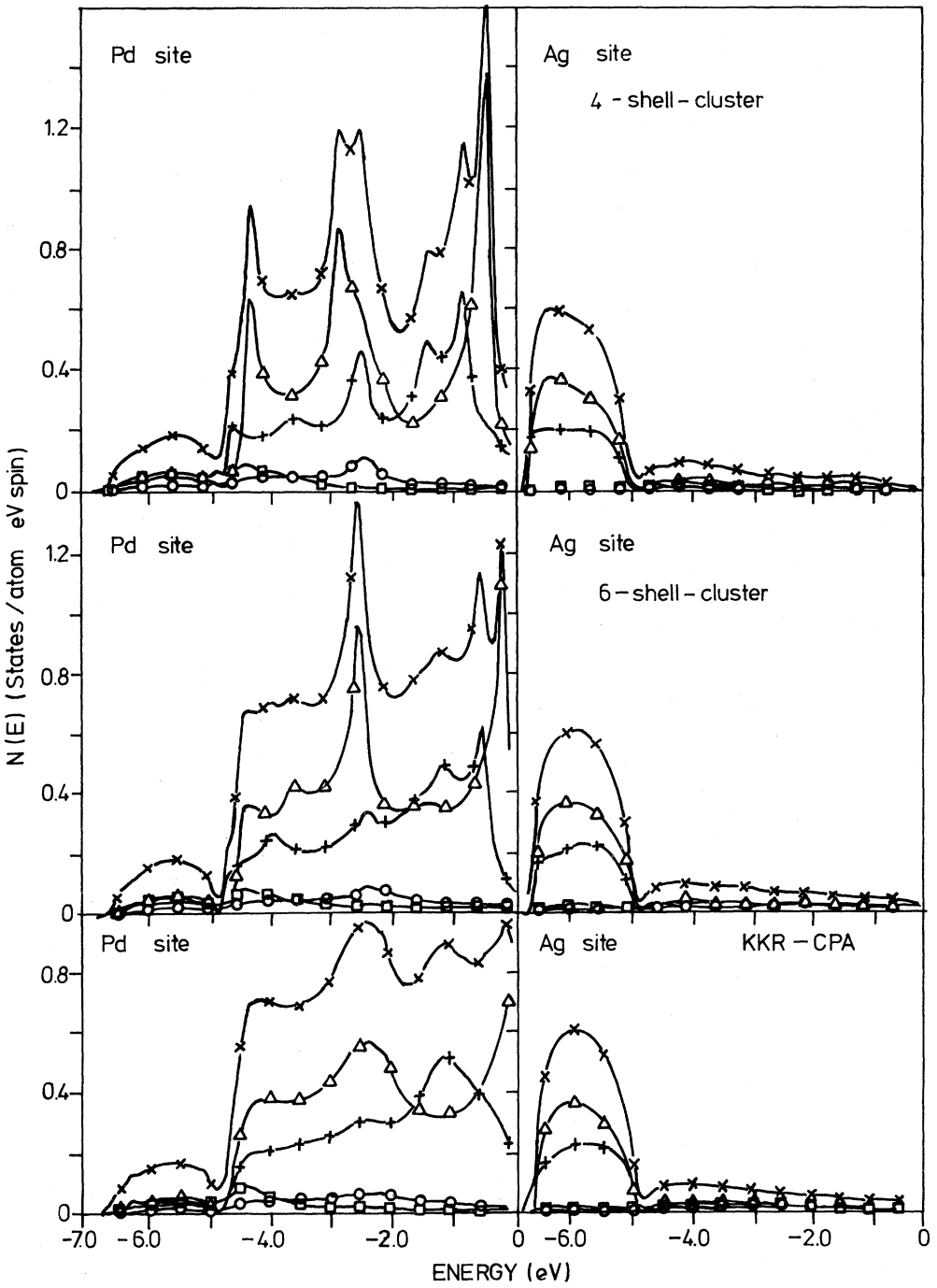

FIG. 7. The partial densities of states for $Ag_{0.2}Pd_{0.8}$ based on the non-self-consistent potentials: □, s DOS; +, e_g DOS; ×, total DOS at the corresponding site; ○, p DOS; △, t_{2g} DOS.

the six-shell-cluster charge densities (Figs. 2–5)—which are practically the same—tell us that the clusters we are dealing with are big enough for the purpose they are used for. Furthermore, we compare the output charge densities of the KKR-CPA calculations to those of the cluster calculations both in the first iteration and in an additional final iteration after the convergence criterion had been met. The results of these comparisons are also displayed in Figs. 2–5 and corroborate the claim that our method is practically equivalent to a procedure which would apply the full KKR-CPA to any step.

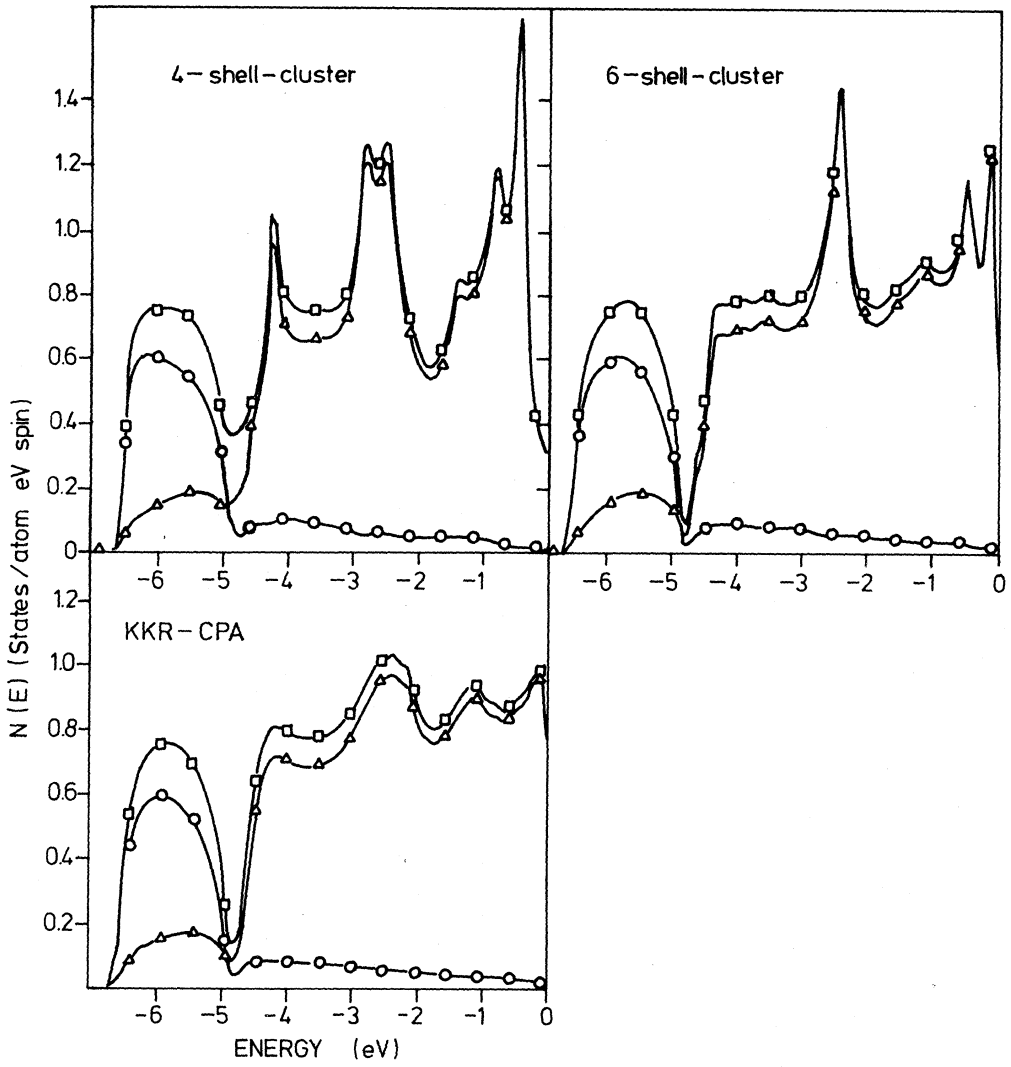

FIG. 8. Total DOS for $Ag_{0.2}Pd_{0.8}$ based on the non-self-consistent potentials: ○, silver site; △, palladium site; □, total DOS. The charge densities of Fig. 2, which are constructed from the quantities displayed in Figs. 7 and 8 coincide in spite of marked differences in the DOS.

These findings are confirmed by the observations made in calculations dealing with other systems too, which will be published elsewhere. The practical identity between the cluster and KKR-CPA charge densities therefore is not fortuitous and limited to the alloy series considered in this paper, but is a general feature. The cause of this is that we are able to treat large clusters whose sizes could still be extended, if necessary. The densities of states of smaller clusters consisting of say 19 sites (3 shells of atoms) is so spiky in the case of the Ag_xPd_{1-x} alloys and similar systems that it would be hard to stabilize the convergence procedure when using them. Furthermore, previous calculations trying to increase the manageable cluster sizes by suppressing *s* and *p* scattering in the Ag_xPd_{1-x} and similar systems, where *d* scattering is predominant, failed to produce reasonable results.

The details of the full KKR-CPA calculations have been given in a host of publications, e.g., in Ref. 6. For the technicalities concerning the KKR-CPA runs we refer the reader to that publication.

As Figs. 3—5 show, the charge densities both at the silver and palladium sites vary smoothly throughout the concentration range. This is true for both the self-consistent and the non-self-consistent results. With increasing Ag concentration the main peaks of the valence charge densities at the silver and palladium sites are slightly shifted towards the ion cores, whereby their peak heights show a small

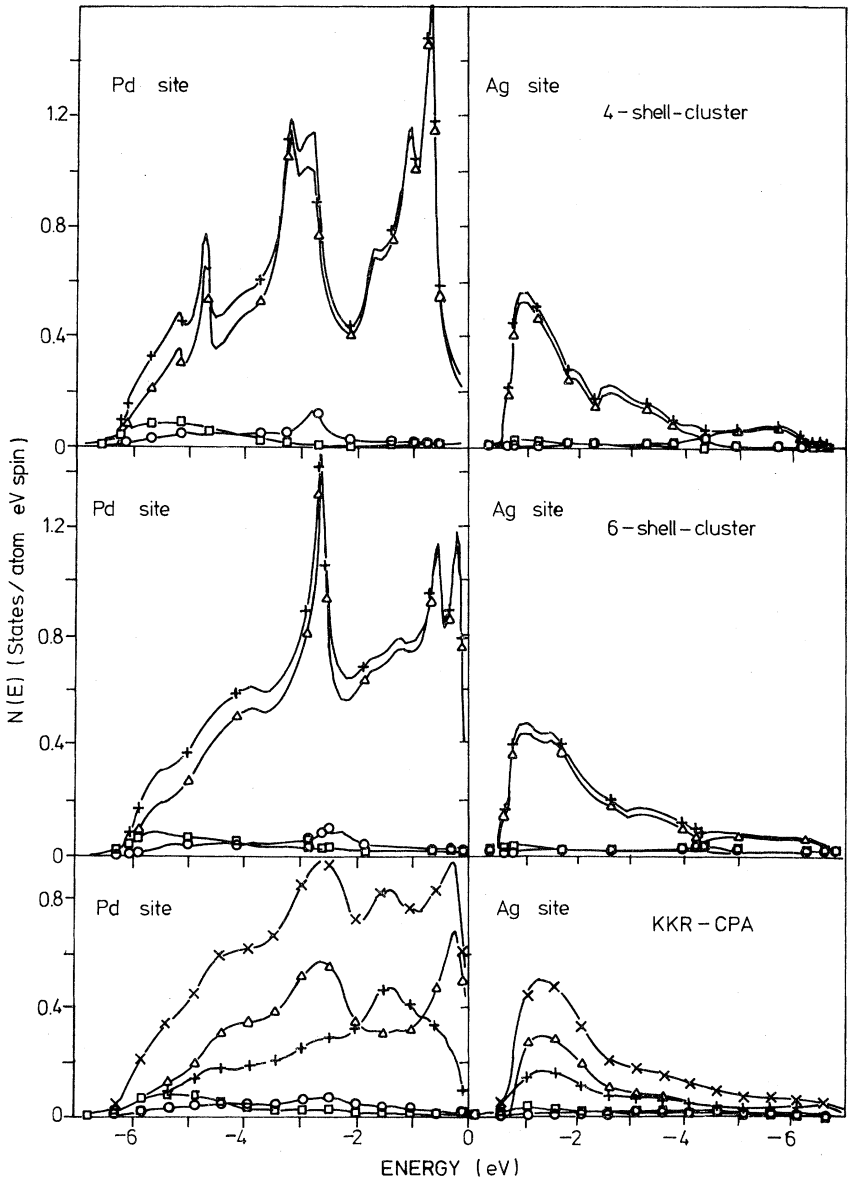

FIG. 9. The self-consistent partial densities of states for $Ag_{0.2}Pd_{0.8}$: □, *s* DOS; ○, *p* DOS; △; *d* DOS; +; total DOS at the corresponding site.

increase. This effect is accompanied by a shift of the *d* resonances to lower energies as one approaches the Ag-rich side in the concentration range (Fig. 6). The aforementioned considerations show that it is unnecessary to repeat the iterations for arbitrary concentrations. All the single-site input quantities required for a KKR-CPA run may be gained by interpolation from those of the three concentrations for which our calculations have been done.

The difference between the self-consistent and the non-self-consistent results can also be seen from Fig. 6. The non-self-consistent phase shifts are identical to those of Ref. 6, whereas our self-consistent phase shifts at the silver sites are shifted up in energy. Because the Pd *d* phase shifts hardly move, this amounts to a reduction in the Ag-Pd *d* band splittings. In $Ag_{0.2}Pd_{0.8}$, e.g., its value is reduced from 5.9 eV for the non-self-consistent case to 5.4 eV for the self-consistent one (compare Figs. 8 and 10). Also reduced are the peak heights of the single-site *d* DOS at the silver sites in accordance with a slight broadening of the Ag *d* resonances. In $Ag_{0.2}Pd_{0.8}$, e.g., this effect is quite pronounced and might be important in the interpretation of XPS spectra, etc.

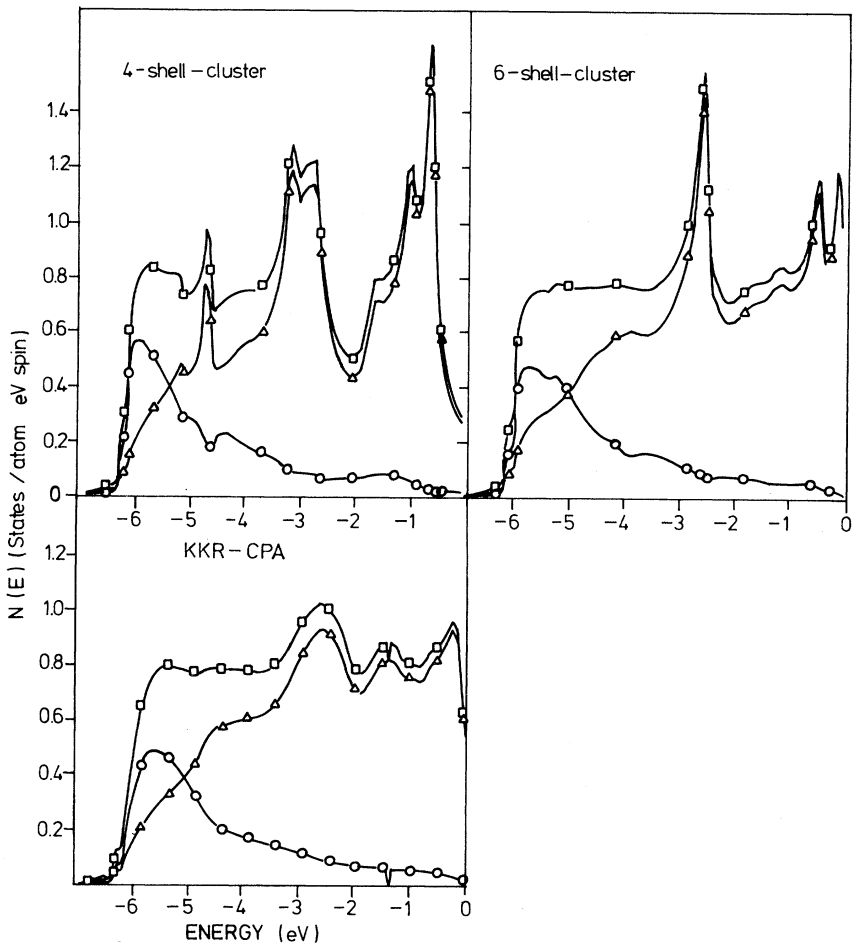

FIG. 10. The self-consistent total DOS for $Ag_{0.2}Pd_{0.8}$: ○, silver site; △, palladium site; □, total DOS. The charge-distributions of Fig. 3 are obtained from the DOS displayed in this figure.

In Figs. 9—15 we present, as examples for electronic-structure quantities self-consistent partial and total DOS for the three compositions and in Figs. 7 and 8 those based on the non-self-consistent potentials for $Ag_{0.2}Pd_{0.8}$. In these figures we compare the four- and six- shell-cluster results to those of the full KKR-CPA calculation. One observes that the results of the bigger clusters are nearer to those of the KKR-CPA. The main difference is that the cluster DOS are more spiky than the KKR-CPA results in the *d*-resonance ranges of the sort of atoms which have the higher concentration in the alloy. The cluster results are nearest to the KKR-CPA results in the $Ag_{0.5}Pd_{0.5}$ case. The scattering at the distant sites tend to wash out the structure in the *d* DOS which may be seen by comparing the four-shell-cluster to the six-shell-cluster results. The full KKR-CPA DOS only show a small indication of the spikes obtained with the clusters. The cluster results, however, agree with the KKR-CPA results in the feature that they place the silver and the palladium *d* resonances at the right positions. Furthermore the *d* band widths of the six-shell clusters agree with those of the KKR-CPA. While with the four-shell cluster the silver *d* bandwidths come out correctly; the Pd *d* band widths are slightly too small. On the whole, however, the clusters are good enough to give the correct charge densities (compare Figs. 3—5). The same conclusion holds for the results based on the non-self-consistent potentials, which are displayed for $Ag_{0.2}Pd_{0.8}$ in Fig. 2 as an example.

In the whole concentration range the silver *d* peaks are well separated from the Pd *d* peaks. The tails of the *d* DOS of one component extend into the *d*-resonance range of the other. In the case of the self-consistent results this leads to a vanishing or at least a reduction of the dips between the *d* resonances for all concentrations. The most pronounced effect occurs in the Pd-rich alloys: In the $Ag_{0.2}Pd_{0.8}$

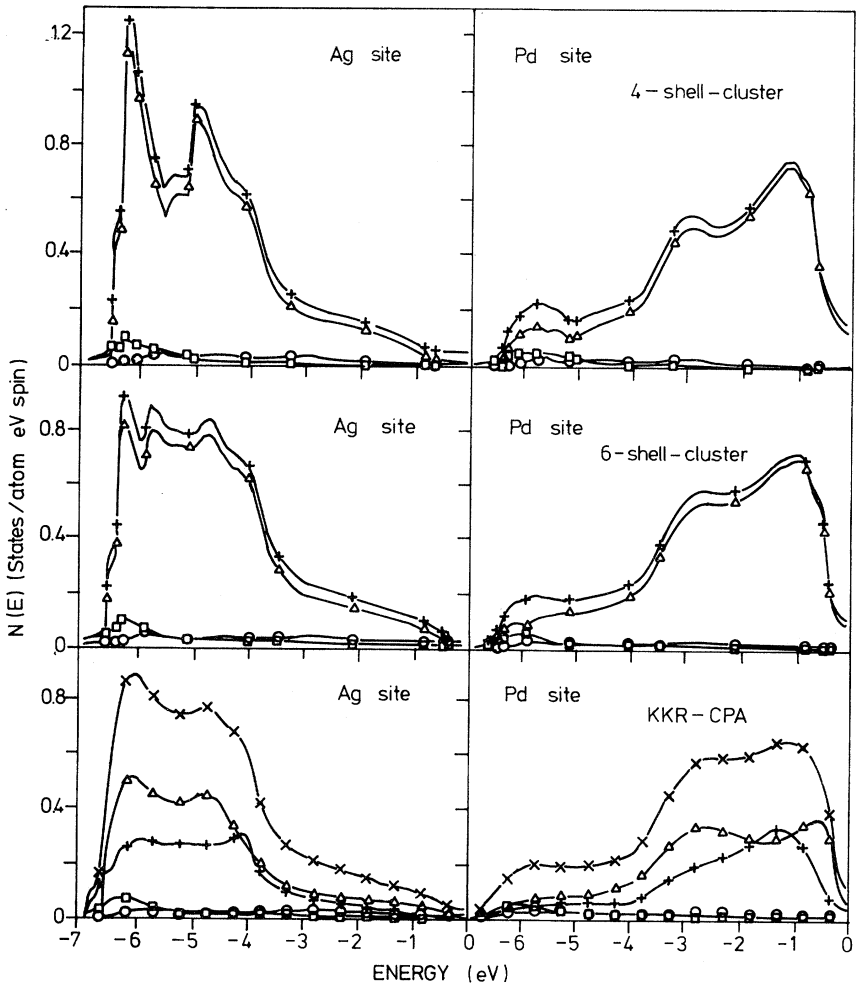

FIG. 11. The self-consistent partial densities of states for $Ag_{0.5}Pd_{0.5}$. The meaning of the symbols is the same as in Fig. 9.

system, e.g., the low-DOS region of the non-self-consistent calculation vanishes in the self-consistent case. This effect is quantified in column 3 of Table IV, where it may also be seen that the agreement in the positions of the d bands between theory and experiment is improved by the self-consistent results.

We are now in the position to calculate all the quantities of interest connected to the self-consistent electronic structure, like electron bands, the shape of the Fermi surface, etc., and compare them to the non-self-consistent results of Ref. 6, which are identical to those recalculated by us. As an example we make this comparison for the Bloch spectral functions $A(\vec{k},\epsilon)$. $A(\vec{k},\epsilon)$ with $\vec{k}$ the momentum vector within the Brillouin zone and ϵ the electron energy has been defined and discussed, e.g., in Ref. 6. In the case of an ordered crystal, when considered as a function of energy at constant $\vec{k}$, its δ-function spikes trace the positions of the electron bands. In the alloy systems we are interested in, these spikes are broadened, signalizing the finite lifetimes of the one-particle states in those systems. As an example we display the Bloch spectral functions based on the self-consistent potentials (Figs. 16–18) for five $\vec{k}$ points in the (1,0,0) directions. They might be contrasted with those based on the Mattheiss prescription potentials as displayed in Ref. 6. An overall comparison between those two groups of results shows marked differences. For example, whereas the non-self-consistent results exhibit gaps between the low-energy structures caused by the silver bands on the one hand and the higher-energy structures due to the palladium bands on the other, the self-consistent results do not. Furthermore in the silver-rich alloys the unstructured peak indicating the Pd-impurity band is narrower and more pro-

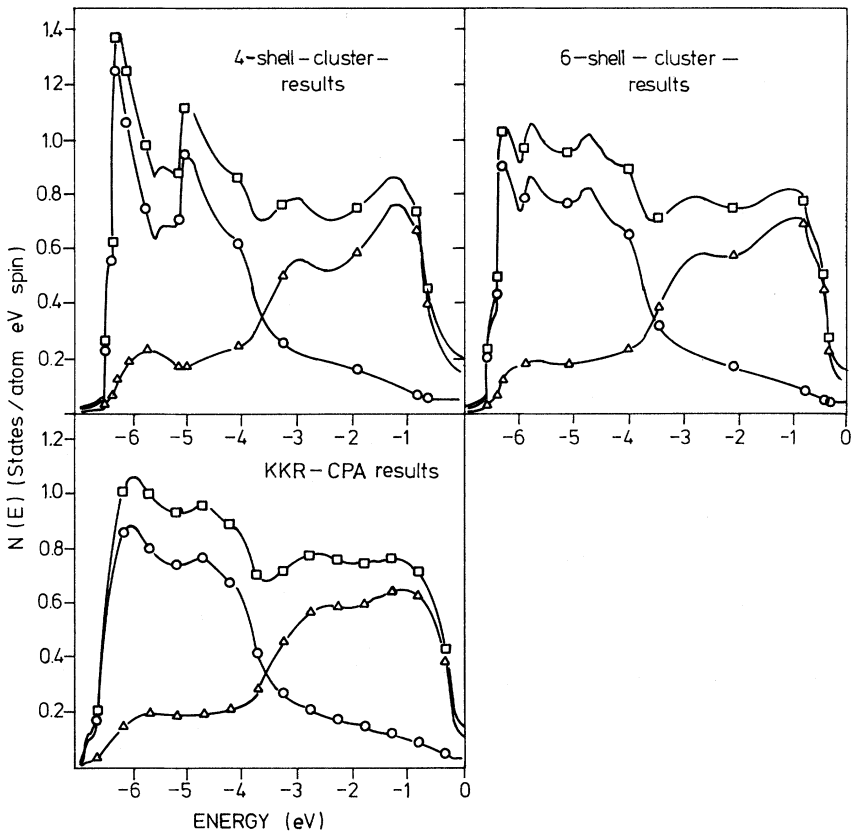

FIG. 12. The self-consistent total DOS for $Ag_{0.5}Pd_{0.5}$. The meaning of the symbols is the same as in Fig. 9. The charge-distribution of Fig. 4 are obtained from the DOS displayed in this figure.

nounced in the self-consistent case. The self-consistent results show more structures for the $Ag_{0.5}Pd_{0.5}$ alloy than the non-self-consistent ones. Furthermore, self-consistency almost obliterates the features found near the gaps of the non-self-consistent results. In addition we observe slight shifts in the positions of the peaks. The examples cited above clearly show that self-consistency causes changes in the broadened bands, which could be probed by performing angle-resolved photoemission experiments.

One might attempt to find a connection between the structures of the Bloch spectral functions and the band structure of the pure system, as Pindor *et al.*[6] did for the non-self-consistent case. This can be achieved nicely for the silver-rich alloy $Ag_{0.8}Pd_{0.2}$ by comparing Fig. 18, to the band structure of the hypothetical Ag metal with the lattice constant of $Ag_{0.8}Pd_{0.2}$ as displayed in Ref. 6 for the (1,0,0) direction: the two lowest peaks on the energy scale at the Γ point [$\vec{k}=(0,0,0)$] are due to Ag $\Gamma_{25'}$ and Γ_{12} bands, respectively, whereas the Γ_1 band is still below the muffin-tin zero and is not contained in Fig. 18. The broad peak between 0.32 and 0.48 Ry corresponds to the Pd-impurity band. At $\vec{k}=(0.25,0,0)$ the Δ_1 band has just come above the muffin-tin zero and the structure between 0.15 and 0.30 Ry is connected with the Δ_1, Δ_2', Δ_5, Δ_1, and Δ_2 bands of pure silver, respectively. The two peaks at $\vec{k}=(0.5,0,0)$ correspond to the Δ_1, and Δ_2' bands on the one hand and the Δ_5, Δ_1, and Δ_2 bands on the other. The $\vec{k}=(0.75,0,0)$ graph exhibits a small splitting between the Δ_1 and Δ_2' bands in the lowest-energy feature, whereas the Δ_2 and Δ_5 peaks are still lumped together. The Δ_1 peak now has split off and moved above the Pd-impurity band. At the zone boundary $\vec{k}=(1,0,0)$ the x_1-x_3 splitting is still more pronounced and the fact that pure Ag has near-neighbor x_2 and x_5 bands is indicated by a shoulder exhibited by the higher peak in Fig. 18. The Δ_1 peak has moved to higher energies and is not contained in our figure.

The self-consistent Bloch spectral function of the palladium-rich alloy $Ag_{0.2}Pd_{0.8}$ (Fig. 16) may be interpreted with the help of Fig. 9 in Ref. 6, where the band structure of pure palladium for the $Ag_{0.2}Pd_{0.8}$

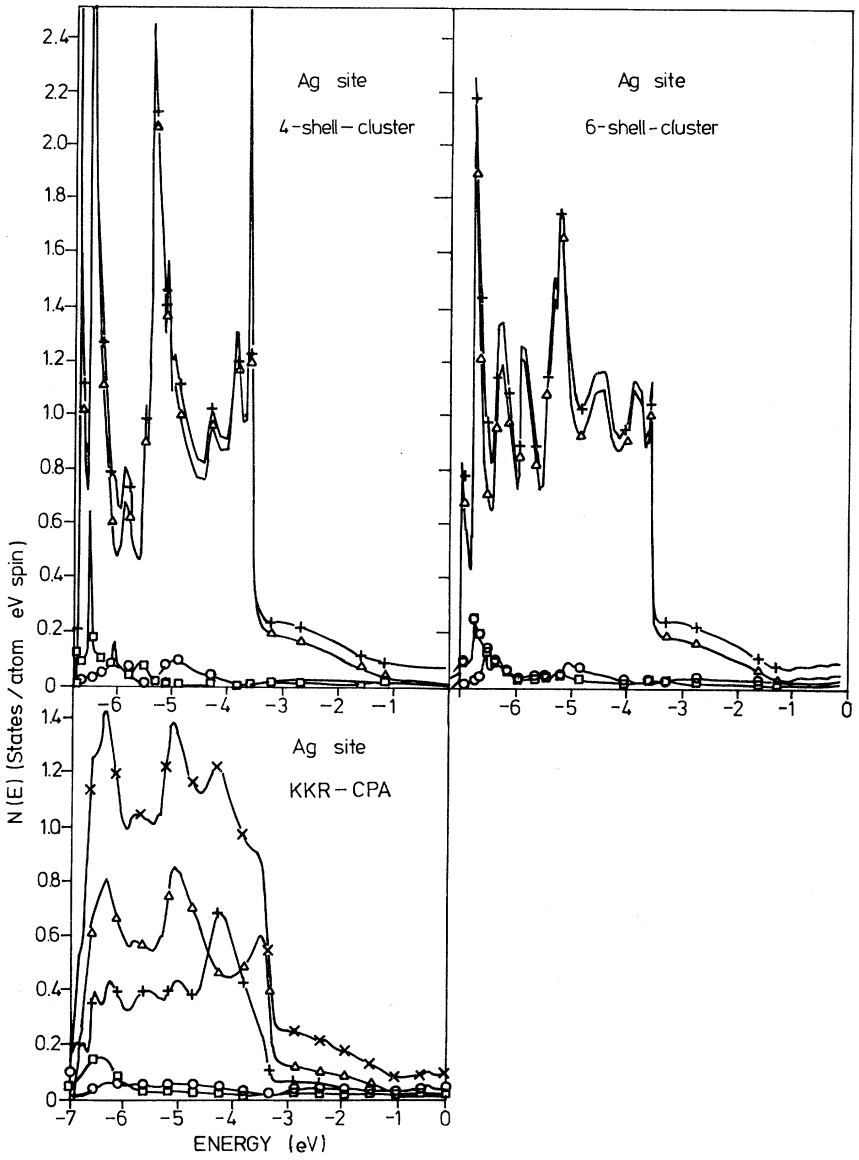

FIG. 13. The self-consistent partial DOS for $Ag_{0.8}Pd_{0.2}$. The symbols are the same as in Fig. 9.

lattice constant is drawn in the (1,0,0) direction: at the Γ point the peaks at 0.35 and 0.47 Ry, respectively, reflect the Γ'_{25} and the Γ_{12} bands of the pure systems, whereas the sharp peak at 0.06 Ry above the muffin-tin zero may be connected with the common Γ_1 band. Farther out in the Brillouin zone, at $\vec{k}=(0.25,0,0)$ the Δ_1 peak is still very narrow, whereas the palladium features between 0.27 and 0.51 Ry show broadening. The lower peak of this structure together with its shoulder corresponds to the slightly split Δ_2 and Δ_5 bands of Pd, whereas the double peak at higher energies might be associated with the Δ'_2 and Δ_1 bands of pure Pd. At $\vec{k}=(0.5,0,0)$ the low-energy peaks are smeared out, whereas the higher-energy peaks, reflecting the Δ_5, Δ_2, and Δ_1 bands of the pure system, sharpen. At $\vec{k}=(0.75,0,0)$ we still encounter the same situation, and at the X point we find extremely narrow peaks, which may be interpreted as the X_1 and X_3 states in the low-energy range on the one side and the X_2 and X_5 states at the aforementioned concentration ranges being more tightly connected with the features of the pure systems than the non-self-consistent results are.

In concluding this section we come back to a point already mentioned above: The differences be-

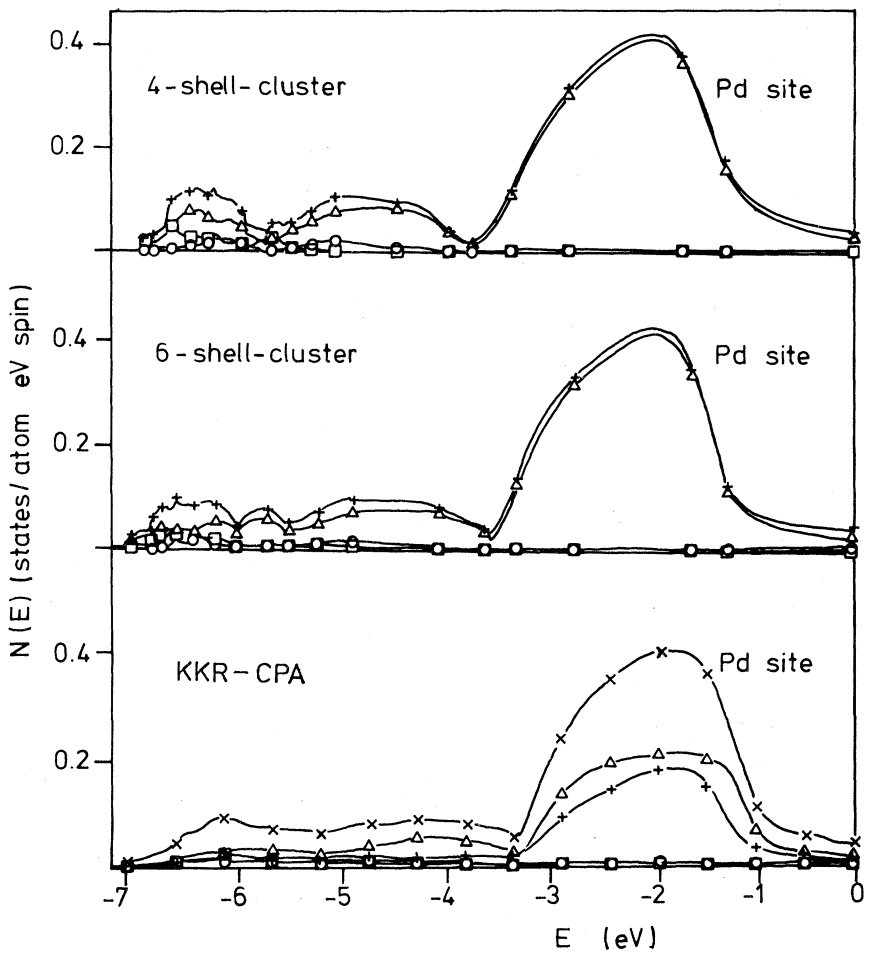

FIG. 14. The self-consistent partial DOS for $Ag_{0.8}Pd_{0.2}$. The symbols are the same as in Fig. 9.

tween our results and those of Ref. 6 are combined self-consistency and exchange-correlation effects. In order to shed some light on their relative significance we constructed the Mattheiss prescription potentials for the $Ag_{0.2}Pd_{0.8}$ system in addition, using the von Barth–Hedin expression for exchange and correlation. The resulting positions of the *d* resonances with respect to the muffin-tin zero are 0.391

TABLE IV. Some results of the self-consistent calculations versus those based on the non-self-consistent potentials. A detailed comparison with the experiments of Ref. 23 requires the inclusion of matrix-element effects.

	Lattice constant	Fermi energy (Ry)		Positions of the *d* bands (eV)					
		Non-self-	Self-	Non-self-consistent		Self-consistent		Experiment	
Composition	(a.u.)	consistent	consistent	Ag site	Pd site	Ag site	Pd site	Ag site	Pd site
$Ag_{0.2}Pd_{0.8}$	7.415	0.577	0.571	5.9	2.4	5.5	2.2	5.4	2.2
$Ag_{0.5}Pd_{0.5}$	7.518	0.544	0.552	5.5	1.9	5.4	1.9	5.4	2.0
$Ag_{0.8}Pd_{0.2}$	7.630	0.542	0.554	5.4	1.7	5.4	1.9	5.5	1.9

	Valence charge in the muffin-tin sphere				Valence charge in the Wigner Seitz cell			
	Non-self-consistent		Self-consistent		Non-self-consistent		Self-consistent	
Composition	Ag site	Pd site	Ag site	Pd site	Ag site	Pd site	Ag site	Pd site
$Ag_{0.2}Pd_{0.8}$	10.394	9.206	10.222	9.230	11.097	9.983	10.926	10.017
$Ag_{0.5}Pd_{0.5}$	10.397	9.284	10.224	9.308	11.015	9.985	10.943	10.057
$Ag_{0.8}Pd_{0.2}$	10.49	9.393	10.278	9.416	10.998	10.01	10.962	10.151

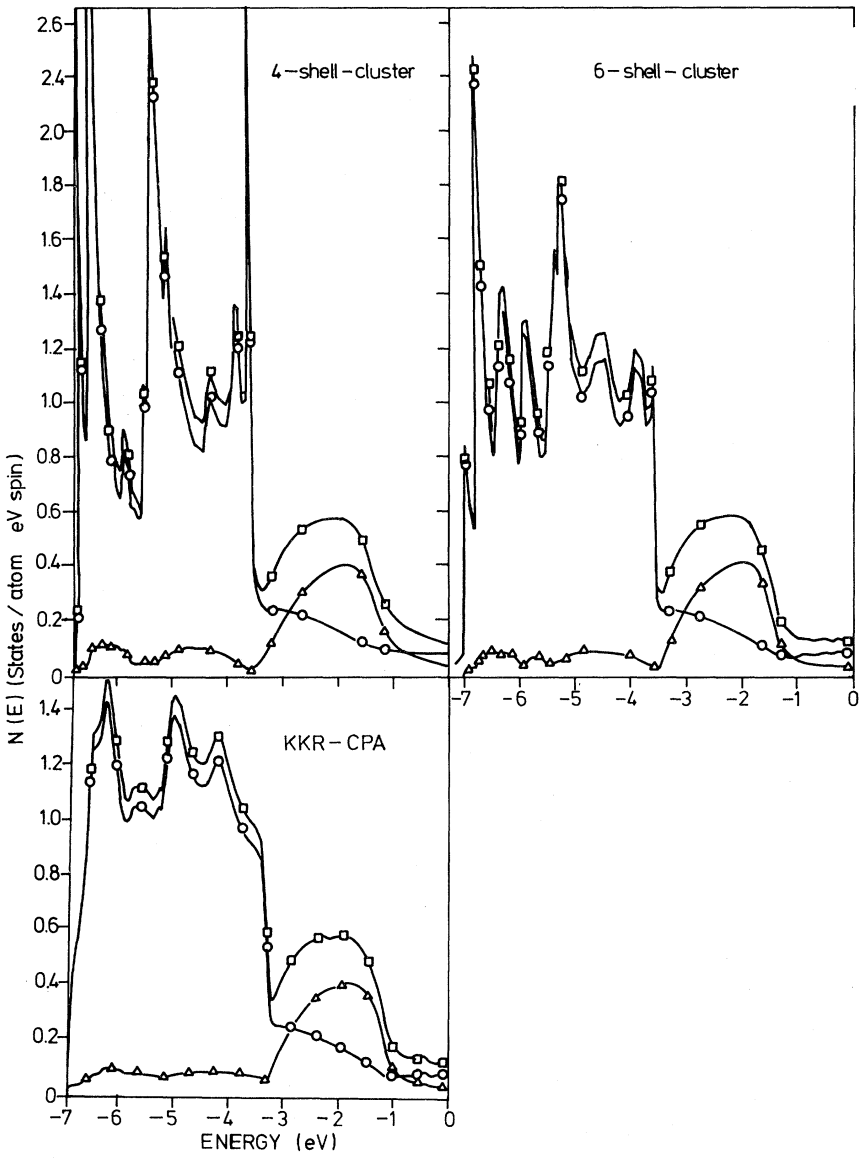

FIG. 15. The self-consistent total DOS for $Ag_{0.8}Pd_{0.2}$. The symbols are the same as in Fig. 10. The charge distributions of Fig. 5 are obtained from the DOS displayed in this figure.

Ry for the Ag and 0.592 Ry for the Pd site. The corresponding numbers of our self-consistent calculations are 0.215 and 0.372 Ry and those of Ref. 6, 0.165 and 0.388 Ry, respectively. We see that both effects are of the same order of magnitude and have different signs in this example. This partial cancellation is the reason why, in the case considered, the $\alpha=1$ Slater exchange leads to better results than the von Barth–Hedin formula when used in a non-self-consistent calculation.

V. SUMMARY

In the present paper we presented a detailed formalism devised for the self-consistent calculation of the electronic structures of substitutionally random alloys in the frame of the KKR-CPA. We demonstrated both the feasibility and the accuracy of our approach by applying it to the Ag_xPd_{1-x} alloy series and performing the necessary numerical computations with the use of both the IBM 3033's at the

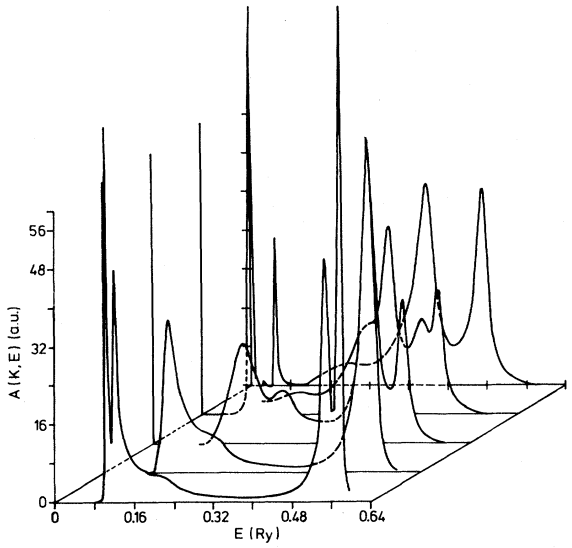

FIG. 16. The Bloch spectral function of $Ag_{0.2}Pd_{0.8}$ for some constant $\vec{k}$ values. Five equidistant $\vec{k}$ points in the (1,0,0) direction are picked out, including the Γ and the χ point. The results are based on our self-consistent potentials.

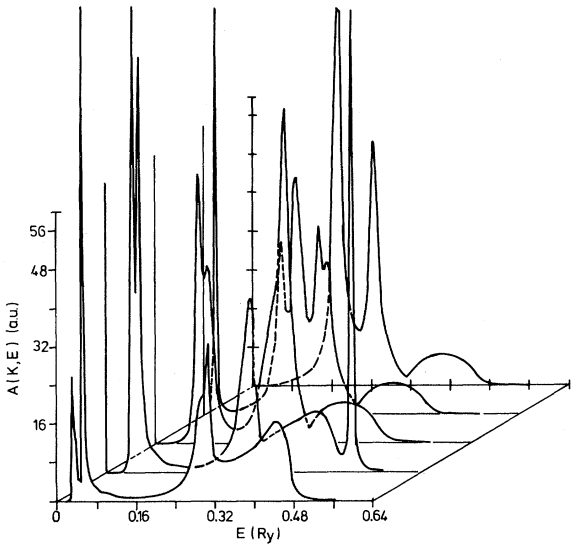

FIG. 18. The Bloch spectral function of $Ag_{0.8}Pd_{0.2}$ for $\vec{k}$ points in the (1,0,0) direction. The results are based on our self-consistent potentials.

Kerforschungszentrum Karlsruhe and the Oak Ridge National Laboratory on the one hand and the Cray at the Science and Engineering Research Council in Daresbury (England) on the other. These experiences lead to the conclusion that our method is able to treat substitutionally random alloys with an amount of expenditure comparable to that required for ordered solids. In addition we pointed out how to include some deviation from complete randomness in our formalism. In spite of the fact that there are a lot of substances for which self-consistency is more important than for the example discussed in the present paper we chose the Ag_xPd_{1-x} system, on account of the availability of the detailed non-self-consistent calculations of Ref. 6 against which our results may be contrasted. Owing to its sensitive and narrow *d* resonances the Ag_xPd_{1-x} system is a genuine test case for the applicability of our method in any case. This statement is also corroborated by the results we obtained by the application of our method to other systems and which will be published elsewhere. Furthermore the experience of others who are using our programs for activities such as those indicated in the Introduction also back our statement above. In addition to their principal character our self-consistent calculations for the Ag_xPd_{x-1} system also bear some physical relevance because they lead to perceptible and measurable modifications of the non-self-consistent results. Whereas the comparison of the positions of the *d* resonances as found in our calculations and displayed in Table IV with the non-self-consistent results of Ref. 6 (Table II in their publication) and with the XPS experiments of Ref. 23 shows improvement of the self-consistent results over the non-self-consistent ones, a detailed discussion of those experiments in terms of our results requires the inclusion of matrix-element effects in our calculations. These computations, which are currently being made and will be published elsewhere show, e.g., that the matrix elements at the silver sites are larger than those at the palladium sites. As a conse-

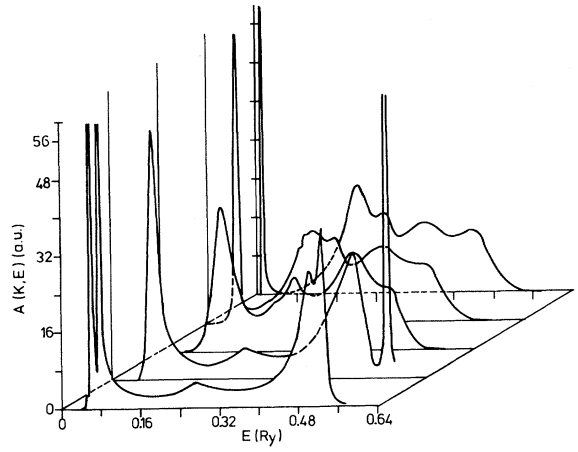

FIG. 17. The Bloch spectral function of $Ag_{0.5}Pd_{0.5}$ for $\vec{k}$ points in the (1,0,0) direction. The results are based on our self-consistent potentials.

quence, dips between the Ag and the Pd *d* resonances occur in the calculated XPS curves even if they are not present or only slightly indicated in the total DOS curves. This feature together with the improvement in the position of the *d* resonances leads us to the expectation that our findings compare favorably to the experiments of Ref. 23. The most useful test of course would consist in a detailed investigation of the band structure, or more precisely the Bloch spectral functions, by angular-resolved photoemission experiments.

ACKNOWLEDGMENTS

We are grateful to Dr. S. Faulkner, Dr. W. Butler, Dr. P. Durham, and Dr. W. Temmerman for their interest in our work and helpful discussions. It is a pleasure to thank the Science and Engineering Research Council of England for giving us the opportunity to use the Cray in Daresbury.

[1]P. Hohenberg and W. Kohn, Phys. Rev. 136B, 864 (1964).
[2]W. Kohn and L. J. Sham, Phys. Rev. 140A, 1133 (1965).
[3]P. Soven, Phys. Rev. 156, 809 (1967).
[4]A. Bansil, L. Schwartz, and H. Ehrenreich, Phys. Rev. B 12, 2893 (1975).
[5]G. M. Stocks, B. L. Gyorffy, E. S. Giuliano, and R. Ruggeri, J. Phys. F 7, 1859 (1977).
[6]A. J. Pindor, W. M. Temmerman, B. L. Gyorffy, and G. M. Stocks, J. Phys. F 10, 2617 (1980).
[7]L. F. Mattheiss, Phys. Rev. B 1, 373 (1970).
[8]G. M. Stocks and W. H. Butler, in *Physics of Transition Metals, 1980,* edited by P. Rhodes (Institute of Physics and Physical Society, London, 1981).
[9]P. J. Durham, D. Ghaleb, B. L. Gyorffy, C. F. Hague, J.-M. Mariot, G. M. Stocks, and W. M. Temmerman, J. Phys. F 9, 1719 (1979).
[10]B. L. Gyorffy, A. Pindor, and W. M. Temmerman, Phys. Rev. Lett. 43, 1343 (1979).
[11]B. L. Gyorffy and G. M. Stocks, J. Phys. F 10, L321 (1980).
[12]P. J. Durham, N. K. Allen, B. L. Gyorffy, J. B. Pendry, and W. Temmerman, in *Physics of Transition Metals 1980,* edited by P. Rhodes (Institute of Physics and Physical Society, London, 1981).
[13]H. Winter and G. M. Stocks, in *Proceedings of the 2nd General Conference of the Condensed Matter Division of the European Physical Society, Europhysics Conference Abstracts,* edited by V. Heine (The European Physical Society, Petit-Lancy 2,1982), Vol. 6A, p. 436.
[14]G. M. Stocks and H. Winter, Z. Phys. B 46, 95 (1982).
[15]G. M. Stocks and W. H. Butler, Phys. Rev. Lett. 48, 55 (1982).
[16]G. M. Stocks and H. Winter (unpublished).
[17]B. L. Gyorffy and G. M. Stocks, Phys. Rev. Lett. (in press).
[18]P. Loyd and P. V. Smith, Adv. Phys. 21, 69 (1972).
[19]J. W. D. Connolly, National Science Foundation Report No. 94 (unpublished).
[20]J. F. Janak, Phys. Rev. B 9, 3985 (1974).
[21]G. Ries and H. Winter, J. Phys. F 9, 1589 (1979).
[22]M. von Barth and L. Hedin, J. Phys. C 5, 1629 (1972).
[23]S. Hüfner, G. K. Wertheim, and J. H. Wernick, Phys. Rev. B 8, 4511 (1973).